ARCHIVES OF ELECTRICAL ENGINEERING VOL. 73(4), pp. 907–926 (2024)

DOI 10.24425/aee.2024.152102

Analytical design of Spoke Internal Permanent Magnet machines using polar-consistent approximation of cubic subdomains

MEISAM POURAHMADI-NAKHLI [1], MASOUD JOKAR KOUHANJANI [2]✉, FARSHAD JAFARI [2], SOMAYEH NAJIBI [2]

[1] *Department of Electrical and Computer Engineering, University of Hormozgan Bandar Abbas, Iran*

[2] *Department of Technical Study, Shiraz Electric Distribution Company Shiraz, Iran*

e-mail: m.pourahmadi@hormozgan.ac.ir, ✉ masoudjokar@hotmail.com, {farshadjafari66/Somayeh.najibi}@gmail.com

(Received: 04.12.2023, revised: 12.11.2024)

Abstract: Finite element modeling is the main tool in the design of internal permanent magnet electric machines for which accurate analytical designs are hard to be developed. Despite the high accuracy, the main drawback of this type of numerical modeling is the immense burden of calculation and time especially for implementation of complex structures. On the other hand, most of the fast analytical methods have been ineffective in accurate modeling of Internal Permanent Magnet (IPM) machines. This inefficiency is due to the complexity of the IPM segments and their inconsistency with other polar subdomains in rotary machines. In this research, one successful approach which divides the inconsistent domains into several polar-consistent subdomains is applied for fast and accurate analytical calculation of the quantities and objective functions. On the basis of this efficient analytical model and by evolutionary optimization tools, the loss and volume of a spoke PM machine are minimized, then the optimal machine is verified satisfactorily by the Finite Element Method (FEM).

Key words: evolutionary optimization, spoke IPM machines design, subdomain analytic modeling

1. Introduction

Designing and optimizing electromagnetic devices benefit greatly from accurate analytical models, offering speed and flexibility compared to numerical FEMs. However, analytical models are constrained by specific conditions and may involve approximations, potentially leading to inaccuracies in estimating electromagnetic quantities for complex structures. In contrast, FEMs

excel in analyzing intricate electric machine structures with high accuracy. Despite this, the substantial computational burden and time required for each scenario make FEMs less favorable compared to fast and reasonably accurate analytical models. Various types of machines with interior PM structures, such as buried, spoke, V-shaped, and multi-layer PMs (PM assisted reluctance machines), pose challenges in direct modeling as a polar subdomain within the cylindrical shape of rotary machines. Nonetheless, analytical design has been employed in studying the mechanical and electrical aspects of interior PM machines. For instance, Weiwen Ye *et al.* [8] conducted a thermal analysis of PM motors for Electric Vehicle (EV) applications, while Chengxu Sun *et al.* [9] proposed a 1-D analytical model for analyzing the noise and vibration of a double-layer PM motor. Additionally, 0-D analytical approaches have been utilized in [10, 11] to minimize average loss and input current using genetic algorithms in a Spoke Internal Permanent Magnet (SIPM) machine. Furthermore, [12] employed 0-D analytical modeling to compare the performance of V-shaped IPM with surface PM structures.

2-D analytical models with significant precision are commonly utilized for surface mounted or surface inset permanent magnet brushless machines, as these surface PM structures can be accurately defined as subdomains in polar coordinates [13]. However, in some studies, internal PM segments have been approximated directly as a single arc-shaped subdomain in polar coordinates for faster, albeit less accurate, 2-D analysis [14–17].

The design of PM electric machines poses a constrained nonlinear optimization problem with numerous parameters [18]. Typically, the design problem is a multi-objective optimization problem with conflicting goals. Due to the complex interrelation of various machine quantities, defining the appropriate objective function is a critical task. In most cases [18], the objectives include minimizing power losses (implying maximum efficiency), cost, volume, and/or mass, while maximizing performance metrics such as minimum cogging torque, harmonics, vibration, and maximum torque density. Constraints may also be imposed on the problem, arising from mechanical (nominal torque and speed) and electrical (voltage level and saturation) requirements, as well as cost, manufacturing, and dimensional limitations. The optimization technique can take various forms, including nonlinear programming approaches like sequential quadratic programming, or evolutionary approaches such as Genetic Algorithms (GAs) [10, 19], Differential Evolution (DE) [20], Particle Swarm Optimization (PSO) [21–23], Ant Colony (AC) [23, 24], Simulated Annealing (SA) [25, 26], Bee Colony (BC) [27], Harmony Search (HS) [28], and many other random search tools.

This research focuses on designing an SIPM motor with minimal loss and size. Its primary contribution lies in utilizing a highly accurate and fast analytical model [13] for calculating objectives and constraints (including teeth flux density and electromagnetic torque limits) to optimize the SIPM machine. The swift and accurate calculation capability of this approach enables the examination of the search power of three powerful evolutionary search tools – GA, PSO, and DE – for optimal design. Additionally, the Finite Element Method (FEM) is utilized for post-design validation.

2. Methodology of analytic modeling

In many brushless machines featuring a spoke magnet configuration, the internal magnet is typically positioned within the rotor iron in a cubic form. However, cubic structures lack consistency with other symmetric polar shapes found in machine domains. This inconsistency

poses a challenge for two-dimensional models aiming to handle both polar and rectangular domains concurrently. To assess the effectiveness of the two-dimensional analytical model in predicting variables of the spoke machine, it is assumed that the internal magnet of the spoke is situated in a rectangular shape within the two-dimensional space of the machine, as depicted in Fig. 1. The following assumptions are taken into account for the two-dimensional analytical modeling of a machine with a rectangular spoke magnet.

- The spoke magnet is assumed to be rectangular and with tangential magnetization in the polar coordinates of the rotor.
- The hub magnet is considered rectangular and its magnetization is radial.
- Magnetic flux density vector includes radial and tangential components. Also, along the z axis, these components are constant.
- Rotor and stator iron have infinite magnetic permeability.
- The end effect and the effect of iron saturation have been neglected.
- The effect of the eddy current reaction is ignored.
- The magnetization of magnets is independent of the radius.

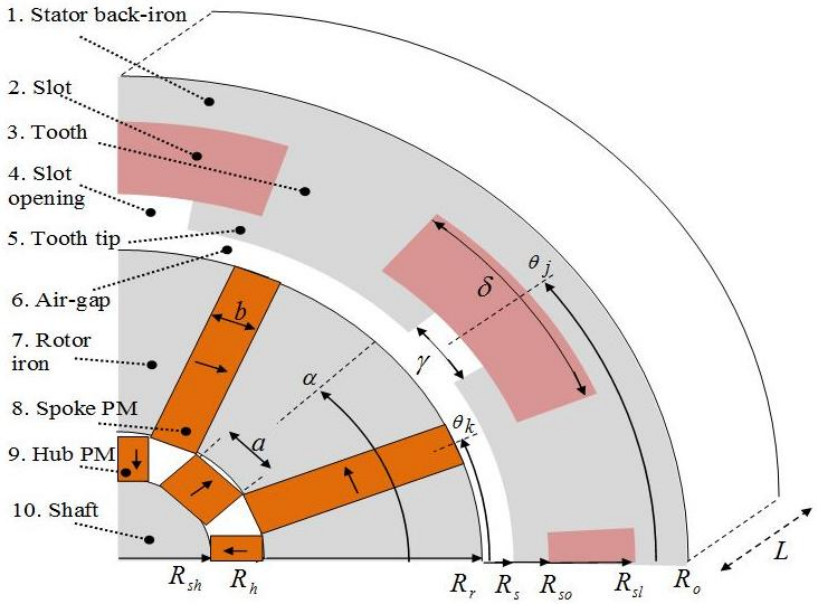

Fig. 1. Cross-section of permanent magnet machine with slotted rectangular spoke with hub magnet

Figure 1 illustrates the stator iron, slot, tooth, slot opening, tooth tip, air gap, rotor iron, spoke magnet, hub magnet, and axis iron, numbered sequentially from 1 to 10. Figure 2 presents the concept of segmenting a rectangular spoke magnet within the polar coordinates of the rotor. To withstand centrifugal forces, rigid non-ferromagnetic retainers encase and secure the hub and spoke magnets, as well as the rotor flux channels, to the shaft.

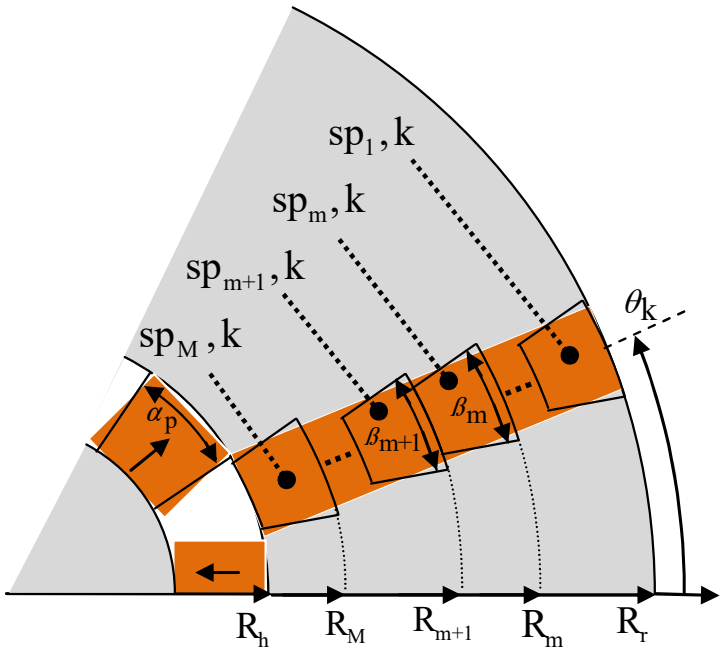

Fig. 2. An approximation of a rectangular spoke magnet with a set of arc-shaped pieces

2.1. Partial Differential Equations (PDEs) of the problem

To apply the two-dimensional analytical model, given the infinite magnetic permeability of stator and rotor iron, the slot sections, slot opening, air gap, spoke magnet, and hub magnet are treated as two-dimensional subdomains. The relationships outlined in the analytical model developed in [13] are employed. According to Maxwell's equations, concerning the magnetic potential vector for each sub-region, we have the following:

$$\frac{\partial^2 A_z^{sl}}{\partial r^2} + \frac{1}{r}\frac{\partial A_z^{sl}}{\partial r} + \frac{1}{r^2}\frac{\partial^2 A_z^{sl}}{\partial \theta^2} = -\mu_0 J_z, \tag{1}$$

$$\frac{\partial^2 A_z^{so}}{\partial r^2} + \frac{1}{r}\frac{\partial A_z^{so}}{\partial r} + \frac{1}{r^2}\frac{\partial^2 A_z^{so}}{\partial \theta^2} = 0, \tag{2}$$

$$\frac{\partial^2 A_z^{a}}{\partial r^2} + \frac{1}{r}\frac{\partial A_z^{a}}{\partial r} + \frac{1}{r^2}\frac{\partial^2 A_z^{a}}{\partial \theta^2} = 0, \tag{3}$$

$$\frac{\partial^2 A_z^{sp}}{\partial r^2} + \frac{1}{r}\frac{\partial A_z^{sp}}{\partial r} + \frac{1}{r^2}\frac{\partial^2 A_z^{sp}}{\partial \theta^2} = -\frac{\mu_0}{r}\left(M_\theta^{sp} - \frac{\partial M_r^{sp}}{\partial \theta}\right), \tag{4}$$

$$\frac{\partial^2 A_z^{h}}{\partial r^2} + \frac{1}{r}\frac{\partial A_z^{h}}{\partial r} + \frac{1}{r^2}\frac{\partial^2 A_z^{h}}{\partial \theta^2} = -\frac{\mu_0}{r}\left(M_\theta^{h} - \frac{\partial M_r^{h}}{\partial \theta}\right), \tag{5}$$

where *sp*, *a*, *so*, *sl* and *h* indicate the subspaces of the spoke magnet, air gap, slot opening, slot and hub magnet, respectively. The boundary conditions of the problem are given in Table 1.

2.2. General solutions

The general solutions satisfying Eqs. (1) to (5) according to the boundary conditions for different subspaces are as follows [13]:

$$\begin{aligned} A_z^{sl,j}(r,\theta) &= a_0^{sl,j} + \frac{\mu_0 j_0^j}{4}\left(2R_{sl}^2 \ln r - r^2\right) \\ &+ \sum_{n=1}^{N} r\left\{ b_n^{sl,j}\left(\left(\frac{R_{so}}{R_{sl}}\right)^{\frac{n\pi}{\delta}+1}\left(\frac{r}{R_{sl}}\right)^{\frac{n\pi}{\delta}-1} + \left(\frac{R_{so}}{r}\right)^{\frac{n\pi}{\delta}+1}\right)\right. \\ &\left. + \frac{\mu_0 j_n^j}{\left(\frac{n\pi}{\delta}\right)^2 - 4}\left(r - \frac{2R_{sl}}{\frac{n\pi}{\delta}}\left(\frac{r}{R_{sl}}\right)^{\frac{n\pi}{\delta}-1}\right)\right\}\cos\left(\frac{n\pi}{\delta}\left(\theta - \theta_j + \frac{\delta}{2}\right)\right), \end{aligned} \tag{6}$$

$$\begin{aligned} A_z^{so,j}(r,\theta) &= a_0^{so,j} + b_0^{so,j}\ln r + \sum_{u=1}^{U} r\left(a_u^{so,j}\left(\frac{r}{R_{so}}\right)^{\frac{u\pi}{\gamma}-1} + b_u^{so,j}\left(\frac{R_s}{r}\right)^{\frac{u\pi}{\gamma}+1}\right) \\ &\times\cos\left(\frac{u\pi}{\gamma}\left(\theta - \theta_j + \frac{\gamma}{2}\right)\right), \end{aligned} \tag{7}$$

$$\begin{aligned} A_z^{a}(r,\theta) &= a_0^a + \sum_{v=1}^{V} r\left(a_v^a\left(\frac{r}{R_s}\right)^{v-1} + b_v^a\left(\frac{R_r}{r}\right)^{v+1}\right)\cos(v\theta) \\ &+ r\left(c_v^a\left(\frac{r}{R_s}\right)^{v-1} + d_v^a\left(\frac{R_r}{r}\right)^{v+1}\right)\sin(v\theta), \end{aligned} \tag{8}$$

$$\begin{aligned} A_z^{sp_m,k}(r,\theta) &= \left\{a_0^{sp_m,k} + b_0^{sp_m,k}\ln r + \sum_{n_m=1}^{N_m} r\left(a_n^{sp_m,k}\left(\frac{r}{R_m}\right)^{\frac{n_m\pi}{\beta_m}-1} + b_n^{sp_m,k}\left(\frac{R_{m+1}}{r}\right)^{\frac{n_m\pi}{\beta_m}+1}\right)\right. \\ &\left.\times\cos\left(\frac{n_m\pi}{\beta_m}\left(\theta - \theta_k + \frac{\beta_m}{2}\right)\right)\right\} + k_p^{sp_m,k} r, \end{aligned} \tag{9}$$

$$\begin{aligned} A_z^{h}(r,\theta) &= \sum_{u=1}^{U} r\left\{a_u^h\left(\left(\frac{r}{R_h}\right)^{u-1} + \left(\frac{R_{sh}}{R_h}\right)^{u-1}\left(\frac{R_{sh}}{r}\right)^{u+1}\right) - \zeta_u^h\left(\frac{R_{sh}}{r}\right)^{u+1} - k_u^h\right\}\sin(u\alpha)\cos(u\theta) \\ &+ r\left\{c_u^h\left(\left(\frac{r}{R_h}\right)^{u-1} + \left(\frac{R_{sh}}{R_h}\right)^{u-1}\left(\frac{R_{sh}}{r}\right)^{u+1}\right) + \zeta_u^h\left(\frac{R_{sh}}{r}\right)^{u+1} + k_u^h\right\}\cos(u\alpha)\sin(u\theta), \end{aligned} \tag{10}$$

which in relations (9) and (10) gives:

$$\zeta_{v1}^s = \frac{R_s \mu_0 J_v^s}{v}\begin{cases} \dfrac{2}{v^2-4} & v \neq 2 \\ -\dfrac{2\ln R_s + 1}{4} & v = 2 \end{cases}, \tag{11}$$

$$\zeta_{v1}^c = \frac{R_s \mu 0 J_v^c}{v}\begin{cases} \dfrac{2}{v^2-4} & v \neq 2 \\ -\dfrac{2\ln R_s + 1}{4} & v = 2 \end{cases}, \tag{12}$$

$$\zeta_u^h = \mu_0 \begin{cases} \dfrac{M_{ru}^h + uM_{\theta u}^h}{u^2 - 1} & u \neq 1 \\ -\dfrac{M_{ru}^h + M_{\theta u}^h}{2}(1 + \ln(R_{sh})) + M_{\theta u}^h & u = 1 \end{cases}. \tag{13}$$

To derive the machine quantities, the unknown coefficients in the general solutions need to be computed initially. This involves utilizing the boundary conditions outlined in Table 1 and employing the method of harmonic equalization across two environments at their shared boundary. The coefficients of the general solutions can be determined through this process. Table 1 provides the boundary conditions formulated based on integral equations. Solving the resulting linear equations and identifying the constants of the general solutions allow for the calculation of all electromagnetic quantities of the machine.

Table 1. Integral coefficients resulting from boundary conditions

Boundary conditions
$$\frac{1}{\gamma}\int_{\theta_j-\gamma/2}^{\theta_j+\gamma/2} A_z^{sl,j}(R_{so},\theta)\,\mathrm{d}\theta = \frac{1}{\gamma}\int_{\theta_j-\gamma/2}^{\theta_j+\gamma/2} A_z^{so,j}(R_{so},\theta)\,\mathrm{d}\theta \tag{14}$$
$$\frac{2}{\gamma}\int_{\theta_j-\gamma/2}^{\theta_j+\gamma/2} A_z^{sl,j}(R_{so},\theta)\cos\frac{\pi u}{\gamma}\theta\,\mathrm{d}\theta = \frac{2}{\gamma}\int_{\theta_j-\gamma/2}^{\theta_j+\gamma/2} A_z^{so,j}(R_{so},\theta)\cos\frac{\pi u}{\gamma}\theta\,\mathrm{d}\theta \tag{15}$$
$$\frac{1}{\delta}\int_{\theta_j-\delta/2}^{\theta_j+\delta/2} H_\theta^{sl,j}(R_{so},\theta)\,\mathrm{d}\theta = \frac{1}{\delta}\int_{\theta_j-\gamma/2}^{\theta_j+\gamma/2} H_\theta^{so,j}(R_{so},\theta)\,\mathrm{d}\theta \tag{16}$$
$$\frac{2}{\delta}\int_{\theta_j-\delta/2}^{\theta_j+\delta/2} H_\theta^{sl,j}(R_{so},\theta)\cos\frac{\pi n}{\delta}\theta\,\mathrm{d}\theta = \frac{2}{\delta}\int_{\theta_j-\gamma/2}^{\theta_j+\gamma/2} H_\theta^{so,j}(R_{so},\theta)\cos\frac{\pi n}{\delta}\theta\,\mathrm{d}\theta \tag{17}$$
$$\frac{1}{\gamma}\int_{\theta_j-\gamma/2}^{\theta_j+\gamma/2} A_z^{a}(R_s,\theta)\,\mathrm{d}\theta = \frac{1}{\gamma}\int_{\theta_j-\gamma/2}^{\theta_j+\gamma/2} A_z^{so,j}(R_s,\theta)\,\mathrm{d}\theta \tag{18}$$
$$\frac{2}{\gamma}\int_{\theta_j-\gamma/2}^{\theta_j+\gamma/2} A_z^{a}(R_s,\theta)\cos\frac{\pi u}{\gamma}\theta\,\mathrm{d}\theta = \frac{2}{\gamma}\int_{\theta_j-\gamma/2}^{\theta_j+\gamma/2} A_z^{so,j}(R_s,\theta)\cos\frac{\pi u}{\gamma}\theta\,\mathrm{d}\theta \tag{19}$$
$$\frac{2}{\pi}\int_{-\pi}^{\pi} H_\theta^{a}(R_s,\theta)\cos\nu\theta\,\mathrm{d}\theta = \frac{2}{\pi}\sum_j\int_{\theta_j-\gamma/2}^{\theta_j+\gamma/2} H_\theta^{so,j}(R_s,\theta)\cos\nu\theta\,\mathrm{d}\theta \tag{20}$$

$$\frac{2}{\pi}\int_{-\pi}^{\pi} H_\theta^a(R_s,\theta)\sin\nu\theta\,\mathrm{d}\theta = \frac{2}{\pi}\sum_j \int_{\theta_j-\gamma/2}^{\theta_j+\gamma/2} H_\theta^{so,j}(R_s,\theta)\sin\nu\theta\,\mathrm{d}\theta \tag{21}$$

$$\frac{1}{\beta_1}\int_{\theta_k-\beta_1/2}^{\theta_k+\beta_1/2} A_z^a(R_r,\theta)\,\mathrm{d}\theta = \frac{1}{\beta_1}\int_{\theta_k-\beta_1/2}^{\theta_k+\beta_1/2} A_z^{sp_1,k}(R_r,\theta)\,\mathrm{d}\theta \tag{22}$$

$$\frac{2}{\beta_1}\int_{\theta_k-\frac{\beta_1}{2}}^{\theta_k+\frac{\beta_1}{2}} A_z^a(R_r,\theta)\cos\frac{\pi n_1}{\beta_1}\theta\,\mathrm{d}\theta = \frac{2}{\beta_1}\int_{\theta_k-\beta_1/2}^{\theta_k+\beta_1/2} A_z^{sp_1,k}(R_r,\theta)\cos\frac{\pi n_1}{\beta_1}\theta\,\mathrm{d}\theta \tag{23}$$

$$\frac{2}{\pi}\int_{-\pi}^{\pi} H_\theta^a(R_r,\theta)\cos\nu\theta\,\mathrm{d}\theta = \frac{2}{\pi}\sum_k \int_{\theta_k-\beta_1/2}^{\theta_k+\beta_1/2} H_\theta^{sp_1,k}(R_r,\theta)\cos\nu\theta\,\mathrm{d}\theta \tag{24}$$

$$\frac{2}{\pi}\int_{-\pi}^{\pi} H_\theta^a(R_r,\theta)\sin\nu\theta\,\mathrm{d}\theta = \frac{2}{\pi}\sum_k \int_{\theta_k-\beta_1/2}^{\theta_k+\beta_1/2} H_\theta^{sp_1,k}(R_r,\theta)\sin\nu\theta\,\mathrm{d}\theta \tag{25}$$

$$\frac{1}{\beta_m}\int_{\theta_k-\beta_m/2}^{\theta_k+\beta_m/2} A_z^{sp_m,k}(R_{m+1},\theta)\,\mathrm{d}\theta = \frac{1}{\beta_m}\int_{\theta_k-\beta_m/2}^{\theta_k+\beta_m/2} A_z^{sp_{m+1},k}(R_{m+1},\theta)\,\mathrm{d}\theta \tag{26}$$

$$\frac{2}{\beta_m}\int_{\theta_k-\frac{\beta_m}{2}}^{\theta_k+\frac{\beta_m}{2}} A_z^{sp_m,k}(R_{m+1},\theta)\cos\frac{\pi n_m}{\beta_m}\theta\,\mathrm{d}\theta = \frac{2}{\beta_m}\int_{\theta_k-\beta_m/2}^{\theta_k+\beta_m/2} A_z^{sp_{m+1},k}(R_{m+1},\theta)\cos\frac{\pi n_m}{\beta_m}\theta\,\mathrm{d}\theta \tag{27}$$

$$\frac{1}{\beta_{m+1}}\int_{\theta_k-\frac{\beta_m}{2}}^{\theta_k+\frac{\beta_m}{2}} H_\theta^{sp_m,k}(R_{m+1},\theta)\,\mathrm{d}\theta = \frac{1}{\beta_{m+1}}\int_{\theta_k-\beta_{m+1}/2}^{\theta_k+\beta_{m+1}/2} H_\theta^{sp_{m+1},k}(R_{m+1},\theta)\,\mathrm{d}\theta \tag{28}$$

$$\begin{aligned}\frac{2}{\beta_{m+1}}\int_{\theta_k-\frac{\beta_m}{2}}^{\theta_k+\frac{\beta_m}{2}} H_\theta^{sp_m,k}(R_{m+1},\theta)\cos\frac{\pi n_{m+1}}{\beta_{m+1}}\theta\,\mathrm{d}\theta \\ = \frac{2}{\beta_{m+1}}\int_{\theta_k-\beta_{m+1}/2}^{\theta_k+\beta_{m+1}/2} H_\theta^{sp_{m+1},k}(R_{m+1},\theta)\cos\frac{\pi n_{m+1}}{\beta_{m+1}}\theta\,\mathrm{d}\theta\end{aligned} \tag{29}$$

$$\frac{1}{\beta_M}\int_{\theta_k-\beta_M/2}^{\theta_k+\beta_M/2} A_z^h(R_h,\theta)\,\mathrm{d}\theta = \frac{1}{\beta_M}\int_{\theta_k-\beta_M/2}^{\theta_k+\beta_M/2} A_z^{sp_M,k}(R_h,\theta)\,\mathrm{d}\theta \tag{30}$$

$$\frac{2}{\beta_M}\int_{\theta_k-\frac{\beta_M}{2}}^{\theta_k+\frac{\beta_M}{2}} A_z^h(R_h,\theta)\cos\frac{\pi n_M}{\beta_M}\theta\,\mathrm{d}\theta = \frac{2}{\beta_M}\int_{\theta_k-\beta_M/2}^{\theta_k+\beta_M/2} A_z^{sp_M,k}(R_h,\theta)\cos\frac{\pi n_M}{\beta_M}\theta\,\mathrm{d}\theta \tag{31}$$

$$\frac{1}{\pi}\int_{-\pi}^{\pi} H_\theta^h(R_h,\theta)\,\mathrm{d}\theta = \frac{1}{\pi}\sum_k \int_{\theta_k-\beta_M/2}^{\theta_k+\beta_M/2} H_\theta^{sp_M,k}(R_h,\theta)\,\mathrm{d}\theta \tag{32}$$

$$\frac{2}{\pi}\int_{-\pi}^{\pi} H_\theta^h(R_h,\theta)\cos u\theta\,\mathrm{d}\theta = \frac{2}{\pi}\sum_k \int_{\theta_k-\beta_M/2}^{\theta_k+\beta_M/2} H_\theta^{sp_M,k}(R_h,\theta)\cos u\theta\,\mathrm{d}\theta \tag{33}$$

$$\frac{2}{\pi}\int_{-\pi}^{\pi} H_\theta^h(R_h,\theta)\sin u\theta\,\mathrm{d}\theta = \frac{2}{\pi}\sum_k \int_{\theta_k-\beta_M/2}^{\theta_k+\beta_M/2} H_\theta^{sp_M,k}(R_h,\theta)\sin u\theta\,\mathrm{d}\theta \tag{34}$$

2.3. Electromagnetic torque, power losses and electromotive force

Using Maxwell's method, the electromagnetic torque exerted on the rotor, located at the α position, is calculated as:

$$T(\alpha) = \frac{LR_a^2}{\mu_0}\int_{-\pi}^{\pi}\left(B^a_{r,\mathrm{PM}}B^a_{\theta,\mathrm{PM}} + B^a_{r,\mathrm{AR}}B^a_{\theta,\mathrm{PM}} + B^a_{r,\mathrm{PM}}B^a_{\theta,\mathrm{AR}} + B^a_{r,\mathrm{AR}}B^a_{\theta,\mathrm{AR}}\right)\mathrm{d}\theta', \tag{35}$$

where: L is the axial length, $B^a_{r,\mathrm{PM}}$ and $B^a_{\theta,\mathrm{PM}}$ are the radial and tangential parts of the PM flux at $R_a = (R_w + R_r)/2$. Moreover, $B^a_{r,\mathrm{AR}}$ and $B^a_{\theta,\mathrm{AR}}$ are the radial and tangential parts of the armature reaction flux at R_a. In Eq. (35), the first part which is due to only PM flux is named cogging torque, and the last part which is only due to armature reaction flux is named reluctance torque.

For core loss calculation here, it is assumed that at the synchronous speed of the rotor, rotor flux variation and thus rotor iron loss due to AR is negligible. The stator iron loss by variation of the first harmonics of the flux is calculated as:

$$\begin{aligned}\mathrm{Core\ Losses} = {} & V_{\mathrm{stator}}\left(K_{hys}B^n_{m,st}f + K_{\mathrm{eddy}}B^2_{m,st}f^2\right)\\ & + N_{\mathrm{slot}}V_{\mathrm{tooth}}\left(K_{hys}B^n_{m,\mathrm{tooth}}f + K_{\mathrm{eddy}}B^2_{m,\mathrm{tooth}}f^2\right)\\ & + V_{\mathrm{tooth,tip}}\left(K_{hys}B^n_{m,\mathrm{tooth,tip}}f + K_{\mathrm{eddy}}B^2_{m,\mathrm{tooth,tip}}f^2\right),\end{aligned} \tag{36}$$

$$V_{\mathrm{stator}} = L\left(\pi R_0^2 - \pi R_{sl}^2\right), \tag{37}$$

$$\mathrm{Copper\ Losses} = 3R_\emptyset R_\emptyset^2 = K_J N_t\, L\, A_w^2 J_b^2. \tag{38}$$

where V_{stator}, V_{tooth}, and $V_{\mathrm{tooth,tip}}$ represent the volume of the stator back-iron, tooth and tooth tip according to Fig. 1, K_{hys} and K_{eddy} are the hysteresis and eddy losses' coefficients depending on

lamination and a core type, $B_{m,st}$, $B_{m,\text{tooth}}$ and $B_{m,\text{tooth,tip}}$ are the maximum flux density in the back-iron, tooth and tooth tip. n is Steinmetz's constant, and f is the electrical frequency of rotation. L is the machine axial length, R_o and R_{sl} are shown in Fig. 1, $R_\emptyset$ is the phase winding resistance carrying current $I_\emptyset$. K_J is the constant equalizing the copper losses with current density J_b, and A_w represent the stator wire gauge in mm^2.

In order to calculate the induced stator coil voltage, first, the link flux of each coil of the phase j winding resulting from the magnet is obtained from the following equation.

$$\emptyset_{j,c}(\alpha) = R_s L \int_{-\frac{\theta_c}{2}+\sigma_{j,c}}^{\frac{\theta_c}{2}+\sigma_{j,c}} B_r^a(R_s, \theta')\, \mathrm{d}\theta', \tag{39}$$

$$BEMF_{j,c}(\alpha) = -N_t \omega \frac{\mathrm{d}\emptyset_{j,c}(\alpha)}{\mathrm{d}\alpha}. \tag{40}$$

N_t is the number of turns of each coil and ω is the angular speed of the rotor.

The two-dimensional analytical model considers a slotted motor with a rectangular spoke magnet supplemented by a hub magnet as outlined in Table 2. To enhance accuracy, the spoke magnet is represented by three stacked arcs. In the analytical model, iron pieces are not treated as subdomains, assuming their permeability to be infinite. Similarly, the assumption of infinite magnetic permeability for rotor and stator iron is accommodated by assigning a very large value in the numerical (FEM) method. In this investigation, the stator winding's injection current is presumed to be completely sinusoidal. The calculation and assessment of magnetic flux density in the air gap emerge as the primary considerations for determining electric torque and Back Electromotive Force (EMF).

Table 2. Initial parameters of the SIPM machine

Parameters	**Symbol**	**Unit**	**Electric Machine with spoke PM**	**Parameters**	**Symbol**	**Unit**	**Electric machine with spoke PM**
Number of phases	q	–	3	The outer radius of the hub area	R_h	mm	12
The number of pole pairs	p	–	2	Rotor radius	R_r	mm	40
The number of spoke areas (p2)	Q	–	4	Inner radius of the stator (inner radius of slot opening)	R_s	mm	41
Radial length of spoke rectangle	b	mm	28	Outer radius of slot opening	R_{so}	mm	43

Continued on next page

Table 2 – *Continued from previous page*

Parameters	**Symbol**	**Unit**	**Electric Machine with spoke PM**	**Parameters**	**Symbol**	**Unit**	**Electric machine with spoke PM**
Tangential length of spoke rectangle	a	mm	9.07	The outer radius of the stator slot	R_{sl}	mm	53
The arc angle of the outer sector of the spoke magnet	β_1	rad	–	Phase winding displacement	θ_c	rad	$\pi/3$
The arc angle of the middle sector of the spoke magnet	β_2	rad	–	The number of turns of each stator coil	N_t	–	30
The arc angle of the inner sector of the spoke magnet	β_3	rad	–	The value of the stator slot current density range	J_0	A/mm^2	500 000
The arc angle of the hub magnet	α_p	rad	–	Amplitude of the current density of the slot j of the stator	J_0^j	A/mm^2	$(-1)^j J_0$
Relative magnetic permeability of hub and spoke magnet	μ_r^{sp}, μ_r^h	–	1.045	Stator slot opening arc angle	γ	rad	π/Q 0.6
Residual flux density of hub and spoke magnets	$B_{rem}^{sp} B_{rem}^h$	T	1.1	Stator slot arc angle	δ	rad	π/Q 1.2
shaft radius (inner radius of the hub area)	R_{sh}	mm	7.5				

3. Evolutionary methods in solving optimization problems

Nature-inspired meta-heuristic methods exhibit a wide range of diversity. Notable among these methods are genetic algorithms, differential evolution algorithms, particle aggregation, ant colony optimization, honey bee optimization, cuckoo search, and others. In the present article, three widely

utilized and robust methods – genetic algorithm, differential evolution algorithm, and particle aggregation – are employed to capitalize on their distinct capabilities in addressing optimization problems. While differential evolution is recognized as a potent search technique, it may converge to local optima. Hence, Particle Swarm Optimization (PSO) and Eenetic Algorithms (GAs) are incorporated to exploit their ability to escape local optima and assess whether more optimal solutions can be attained.

4. Optimization of SIPM machine with spoke magnet

The primary objective of analytical models is their application in the optimal design of electric machines. Their notable advantages, such as high calculation speed for objective functions and rapid implementation in optimization programming, distinguish them from cumbersome numerical Finite Element Method (FEM) calculations. In this section, the highly accurate two-dimensional analytical model proposed for precise calculation of SIPM machine quantities, coupled with its significant computational speed compared to the FEM, forms the foundation for solving the optimization problem. This optimization problem encompasses objectives, constraints, and optimization variables. Objectives in electric machine design can vary widely, including reducing machine losses, enhancing efficiency, minimizing volume, lowering fabrication costs, increasing torque, reducing torque ripple, and more. Similarly, constraints can span a broad spectrum of requirements contingent upon the machine's application. Examples include machine volume, operational speed, tooth flux density, allowable cogging torque, output average torque, etc. Optimization variables dictate the objectives, and by appropriately selecting and adjusting them within their allowable range, desired goals can be achieved. For instance, in the design of a permanent magnet machine, optimization control variables may encompass the number of slots, slot opening angle, magnet thickness, magnet length, rotor back iron thickness, stator back iron thickness, slot opening, slot depth, number of pole pairs, and machine diameter-to-length ratio. Given the intricate relationship between quantities and their dependency on machine structural parameters, a reliable calculation model is imperative for the optimization problem. Moreover, meta-heuristic methods emerge as suitable optimizers for problems with expansive search spaces. In this section, optimization is conducted on an SIPM motor with a rectangular spoke magnet utilizing the two-dimensional analytical method elucidated in Section 2. The optimization objective aims to minimize electromagnetic losses, encompassing iron and copper losses, while simultaneously minimizing machine volume to enhance power density. Additionally, the following criteria must be met as constraints in achieving the aforementioned objective.

For the optimization problem:

– The average torque should not be less than 6 Nm.
– The cogging torque should not be more than 10% compared to the average torque.
– The magnetic flux density in the back iron of the stator and teeth should be at most 1.5 T.

The optimization variables comprise the axial length of the machine, axis radius, thickness of the hub area, radial and tangential lengths of the spoke magnet, thickness of the stator back iron, stator slot depth, stator slot opening angle, slot tip opening depth, slot opening angle, and stator current density. The objective function in this optimization problem aims to minimize losses and machine volume. This objective must be pursued while adhering to the constraints outlined in

Table 3 and ensuring that the electromagnetic torque does not fall below the minimum allowed value. Therefore, the constant parameters of the machine necessary to solve the optimization problem are specified in Table 4.

Table 3. Lower and upper limits of optimization variables

Variable	Unit	Lower limit	Upper limit
Axial length of machine L	Cm	10	15
Internal radius of hub area R_h	Cm	0.5	1
Thickness of hub area l_h	Cm	0.2	0.8
The thickness of spoke magnet b	Cm	0.5	1.5
Depth of spoke magnet l_{sp}	Cm	0.2	0.4
Thickness of stator back iron l_{st}	Cm	0.5	1.5
Depth of slot l_{sl}	Cm	0.4	0.8
Depth of slot opening l_{so}	Cm	0.05	0.2
Opening angle of slot γ	Degree	8	15
Opening angle of slot δ	Degree	15	40
Current density in stator J_b	A/mm^2	3	6

Table 4. Constant parameters of optimization

Parameter	Value	Parameter	value
Number of phases q	3	Relative permeability of hub μ_r^h	1.045
Number of pole pairs p	2	Relative permeability of spoke magnet μ_r^{sp}	1.045
Number of spoke magnets Q	4	Residual magnetic flux density B_{rem}^{sp}	1.1
Coil angle θ_c	$\pi/3$	Residual magnetic flux density B_{rem}^h	1.1

The optimization problem is defined as follows:

$$\text{Minimize: } \omega_p P_{\text{loss}} + \omega_v \text{ Volume}, \tag{41}$$

$$\text{Subject to: average } (T_{em}) > 6 \text{ N} \cdot \text{m}, \tag{42}$$

$$\text{Subject to: } \frac{\max(T_{\text{cog}}) - \min(T_{\text{cog}})}{\text{average } (T_{em})} < 0.1, \tag{43}$$

$$\text{Subject to: } B_{\text{back Iron}} < 1.5 \text{ Tesla}, \tag{44}$$

where P_{loss} is the sum of core and copper losses, and Volume indicates the active part volume that is $L\pi R_o^2$. Inequality constraints are added to the objective function as penalty factors. Also, the coefficients ω_p and ω_v are used to equalize the weight of losses and the volume in the calculation of the final objective function; by trial, weighing coefficients are somehow selected to normalize the loss and volume parts of the objective function each within [0–1].

Table 5 presents the results obtained from four times of solving the problem using GA, DE, and PSO methods.

Table 5. Optimal solutions of genetic algorithm, differential evolution, and particle swarm optimization methods

Optimization method	L cm	R_{ih} cm	l_h cm	a cm	b cm	l_{st} cm	l_{sl} cm	l_{so} cm	γ degree	δ degree	J_b A/m^2	Cost value
DE	10	0.5	0.2	0.89	2	1.04	0.4	0.05	8.01	15.01	5 702 290	0.807
	10	0.5	0.2	0.95	2	1.07	0.4	0.05	8.01	15.01	5 597 167	0.809
	10	0.5	0.2	0.87	2	1.1	0.4	0.05	8.01	15.01	5 903 012	0.836
	10	0.5	0.21	0.95	2	1.07	0.4	0.07	8.22	15.01	5 597 167	0.841
GA	10	0.5	0.22	0.88	2	1.4	0.4	0.07	11.88	15.01	5 941 823	0.869
	10.14	0.5	0.31	0.96	2	1.12	0.4	0.05	8.05	15.01	5 398 404	0.887
	10	0.56	0.2	1	2	1.34	0.4	0.09	13.67	16.4	5 571 326	0.961
	10.02	0.5	0.36	1	2	1.28	0.44	0.07	8.01	15.01	5 276 248	0.962
PSO	11.56	0.55	0.26	0.99	2	1.14	0.4	0.06	8.02	19.3	4 582 724	0.993
	10.94	0.5	0.3	0.93	2.03	1.11	0.45	0.12	8.01	18.39	5 038 861	1.036
	10	0.62	0.39	1.07	2.05	1.20	0.4	0.12	8.01	15.01	4 714 504	1.031
	10.19	0.67	0.21	1.03	2.04	1.27	0.41	0.08	11.00	18.62	5 237 303	1.038

Although DE is commonly recognized as a powerful search tool, it may converge to a local optimum. Hence, we incorporated PSO and the GA to leverage their strengths and ascertain if a more optimal solution could be achieved. The results are arranged based on the best solutions obtained. In all methods, the objective function is calculated using the two-dimensional analytical model with the spoke magnet approximated into three polar-consistent pieces. It is evident from the table that the differential evolution algorithm has yielded more optimal solutions compared to the other two algorithms. Consequently, the solution found by DE in the first row is selected as the optimal solution.

5. Evaluation of the optimal SIPM Motor

To ensure that the best solution obtained is indeed optimal, the sensitivity of the cost function is evaluated by individually changing each parameter while keeping all other parameters fixed at the obtained point. This process involves calculating the variations of the objective function. Figure 3 illustrates the variations of the objective function resulting from changes in each of the eleven optimization variables separately. In each test, it is observed that the best solution corresponds to the critical minimum cost variation. Therefore, this point is deemed the optimal solution to the problem. It is notable from Fig. 3 that most of geometric control variables are pushed to their lower limit for optimal design except for thickness Sp, back iron thickness and current density. This behavior is resealable as there is a significant link between redial (axial) depth of machine subdomains and the size (volume). On the other hand, higher values of current

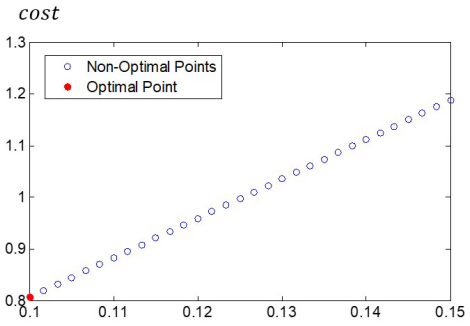

Axial Length (m)

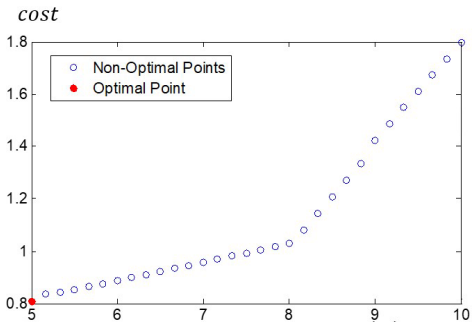

Inner Radiuds of Hub Area (m)

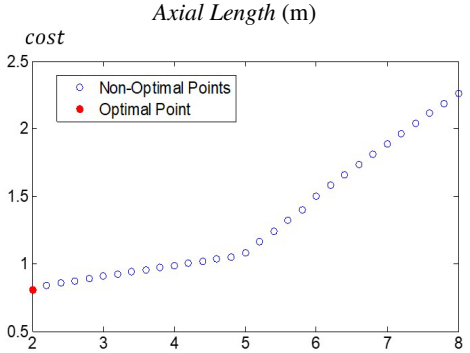

Thickness of Hub Area (m)

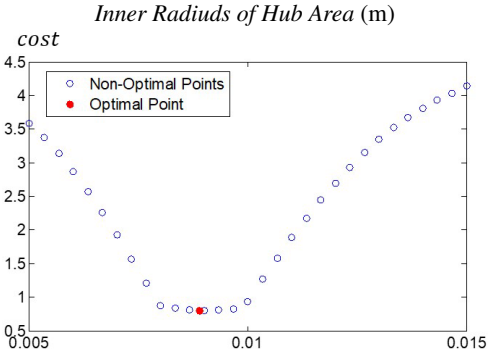

Thickness Spoke Magnet (m)

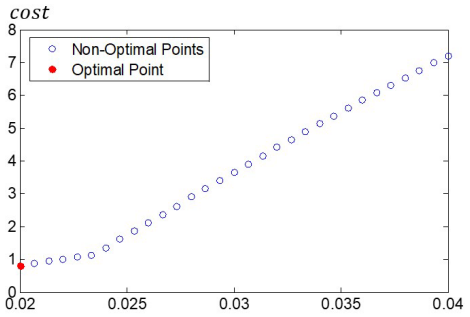

Spoke Depth (m)

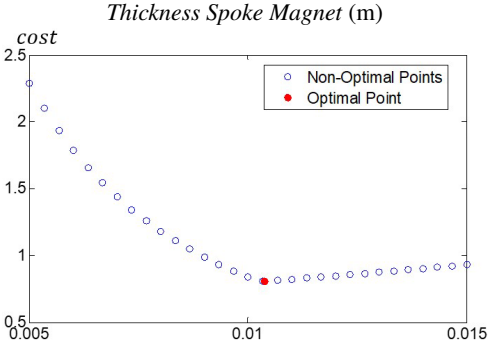

Back Iron Thickness (m)

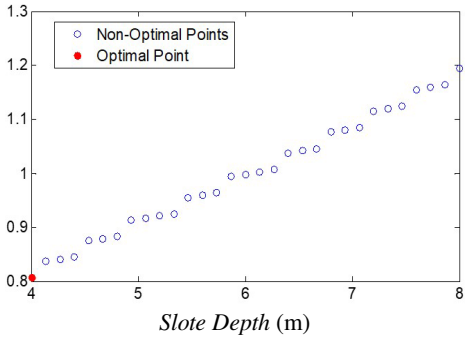

Slote Depth (m)

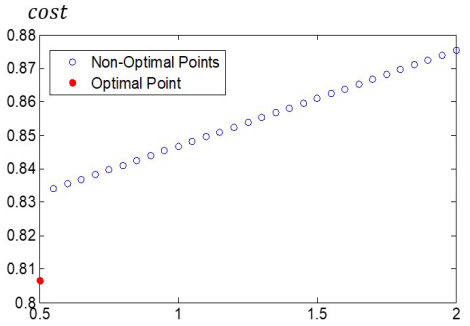

Depth of Slot Opening (m)

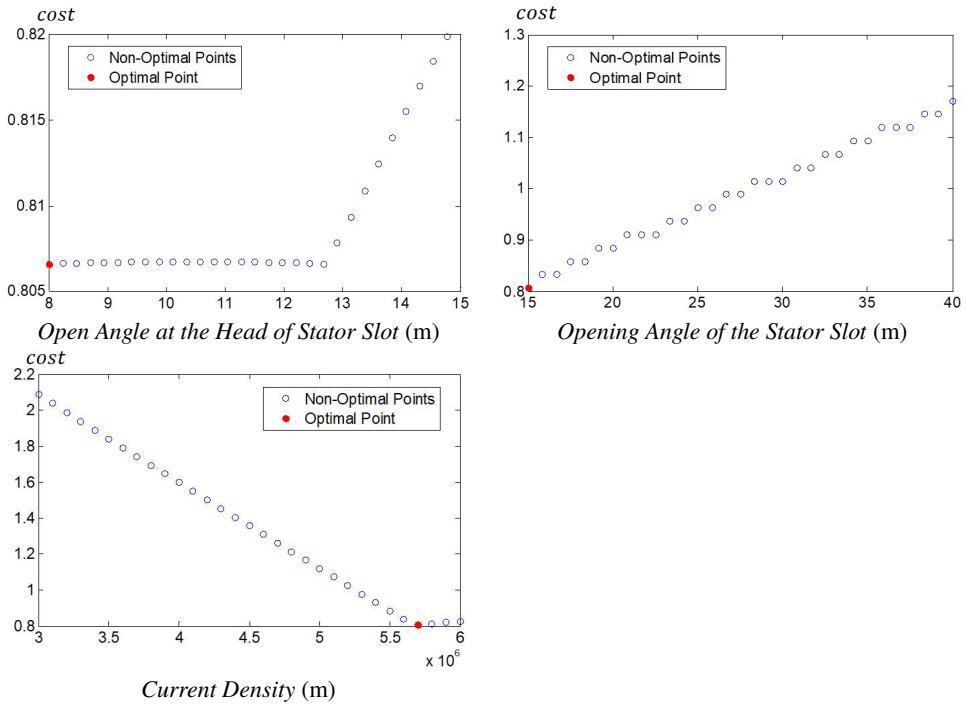

Fig. 3. The changes of the objective function (cost) around the optimal point according to the changes of different optimization variables

density and thickness of a spoke PM can actively satisfy the constrain of the minimum average torque when size is reduced. For further assessment, Table 6 presents the performance of the optimal design in meeting the constraints. The last column of the table indicates that all constraints have been satisfactorily met. One aspect of concern regarding the outputs is the accuracy of the analytical model in calculating the output quantities.

Table 6. Desired objectives at the optimal point and the range of constraints

Variables	Units	Acceptable range	Optimal value
Average electromagnetic Torque	N·m	> 6	6.034
Percentage of cogging torque	N·m	< 10%	0.495%
Maximum cogging flux density	Tesla	< 1.5	0.596
Maximum back iron flux density	Tesla	< 1.5	1.486
Hysteresis losses	Watt	–	1.931
Eddy current losses	Watt	–	0.422
Copper losses	Watt	–	9.117
Volume of machine	cm^3	–	578.2

To assess the reliability of the 2-D analytical model, Finite Element Method (FEM) calculations are conducted at the optimal point, as depicted in Figs. 4 to 6. Figure 4 illustrates the instantaneous torque based on the initial conditions specified in Table 2, while Fig. 5 displays the instantaneous torque and its components under optimal conditions outlined in Table 5 (first row). Both figures confirm that the analytically calculated torque quantities align well with those computed by the FEM. Furthermore, Fig. 6 validates the accurate calculation of flux density components resulting from the permanent magnet (PM) in the middle of the air gap radius, as compared to the FEM calculations.

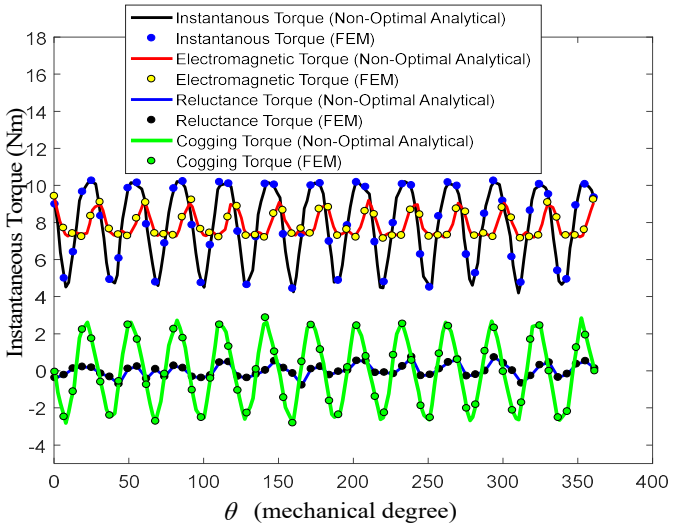

Fig. 4. Instantaneous torque and its different components in initial conditions

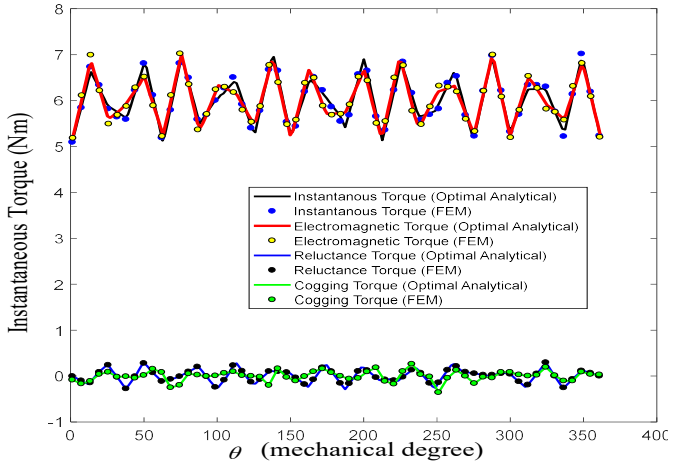

Fig. 5. Instantaneous torque and its various components in optimal conditions

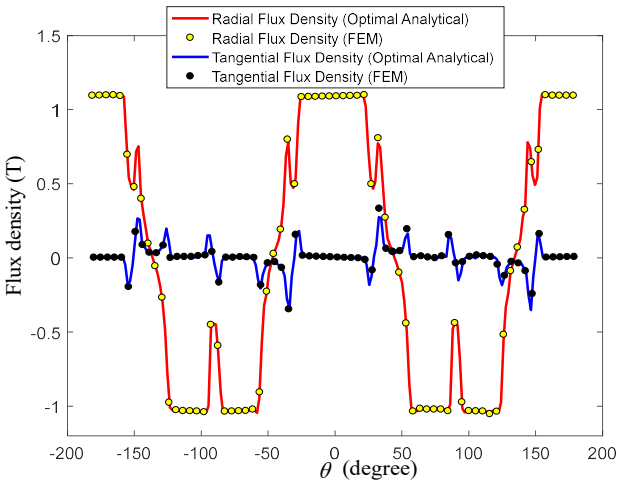

Fig. 6. Airgap flux distribution from magnet, rotor position at $\alpha = 0$

Table 7 provides the specifications of the designed machine. According to the table, the rated power of the motor is 905.1 W, and its efficiency is recorded at 98.75%.

Table 7. Parameters of designed motor

Parameter	**Unit**	**Value**	**Parameter**	**Unit**	**Value**
Number of phases	–	3	Cogging torque percentage	–	0.495
Number of pole pairs	–	2	Maximum flux density at the peak of teeth	tesla	1.808
Number of teeth	–	6	Maximum flux density of teeth	tesla	0.596
Axial length	cm	10	Maximum flux density of stator	tesla	1.486
Radius of machine	cm	8.57	Hysteresis loss	watt	1.931
Inner radius of hub Area	cm	0.5	Eddy current loss	watt	0.422
Thickness of hub	cm	0.2	Copper loss	watt	9.117
Depth of spoke magnet	cm	2	Volume of machine	cm^3	578.2
Thickness of spoke magnet	cm	0.89	Speed	rpm	1500
Thickness of stator back iron	cm	2	Number of rounds per coil	–	7
Depth of slot	cm	0.4	Wire cross section of each coil	mm^2	2
Depth of slot opening	cm	0.05	Coil filling factor	–	0.5
Slot angle	degree	15.01	Stator induced voltage range	volt	6
Slot opening angle	degree	8.01	Average inductance of stator phase	mH	0.3
Stator current density	A/m^2	5702290	Average electromagnetic torque	N·m	6.034
Relative permeability of hub and spoke magnets	–	1.045	Output power	watt	905.1
Residual flux density of hub and spoke magnet	tesla	1.1	Machine efficiency	–	98.75%

Hysteresis losses, eddy current losses, and copper losses account for 16.8%, 3.7%, and 79.5% of the total motor losses, respectively. The notable high efficiency of this motor can be attributed to the excitation by permanent magnets instead of relying on a current-carrying wound rotor. Furthermore, the primary objective of the design is to minimize power loss, which aligns with the goal of increasing efficiency.

6. Conclusion

In this article, an objective function for the machine optimization problem was defined by using the approximation of the rectangular spoke magnet to a set of arc-shaped segments, which has much higher accuracy than other two-dimensional analytical methods of spoke magnet machines. By approximating the rectangular magnet to three arc-shaped layers, high accuracy was obtained in the calculation of electromagnetic quantities compared to the finite element numerical method. This fast and accurate analytical method was used in the optimal design of a slotted SIPM machine. In addition, the search ability of evolutionary methods of the GA, DE and PSO was used and the optimal design with minimum losses and volume was satisfactorily achieved.

References

[1] Bhaktha B. Sandesh, Anil Jogi, Jeyaraj Pitchaimani, Gangadharan K.V., *Design and optimization of an external-rotor switched reluctance motor for an electric scooter*, Materials Today: Proceedings (2023), DOI: 10.1016/j.matpr.2023.03.696.

[2] Zhang G., Yu W., Hua W., Cao R., Qiu H., Guo A., *The Design and Optimization of an Interior, Permanent Magnet Synchronous Machine Applied in an Electric Traction Vehicle Requiring a Low Torque Ripple*, Appl. Sci., vol. 9, 3634 (2019), DOI: 10.3390/app9173634.

[3] Supriya Naik, Baidyanath Bag, Kandasamy Chandrasekaran, *Design optimization of Spoke IPM motor for improving efficiency using PSO and Rao-1 algorithm based FEA*, Materials Today: Proceedings, vol. 80, part 2, pp. 400–408 (2023), DOI: 10.1016/j.matpr.2022.10.188.

[4] Wu H., Zhao W., Zhu G., Li M., *Optimal Design and Control of a Spoke-Type IPM Motor with Asymmetric Flux Barriers to Improve Torque Density*, Symmetry, vol. 14, 1788 (2022), DOI: 10.3390/sym14091788

[5] Pouramin A., Dutta R., Rahman M.F., *Design Optimization of a Spoke-Type FSCW IPM Machine to Achieve Low Torque Ripple and High Torque Density Under a Wide Constant Power Speed Range*, 2018 IEEE Energy Conversion Congress and Exposition (ECCE), Portland, OR, USA, pp. 6914–6921 (2018), DOI: 10.1109/ECCE.2018.8558066.

[6] Demir Y., Ocak O., Aydin M., *Design, optimization and manufacturing of a spoke type interior permanent magnet synchronous motor for low voltage-high current servo applications*, 2013 International Electric Machines & Drives Conference, Chicago, IL, USA, pp. 9–14 (2013), DOI: 10.1109/IEMDC.2013.6556122.

[7] Yoon K.-Y., Hwang K.-Y., *Optimal Design of Spoke-Type IPM Motor Allowing Irreversible Demagnetization to Minimize PM Weight*, in IEEE Access, vol. 9, pp. 65721–65729 (2021), DOI: 10.1109/ACCESS.2021.3070747.

[8] Weiwen Ye, Yongqiu Liu, Guangming Wu, Qifei Wu, Zhensen Chen, Zhensheng Chen, Zhenhua Li, Zhijie Cao, *Design optimization and manufacture of permanent magnet synchronous motor for new energy vehicle*, Energy Reports, vol. 8, Supplement 15, pp. 631–641 (2022), DOI: 10.1016/j.egyr.2022.10.136.

[9] Chengxu Sun, Qi Li, Tao Fan, Xuhui Wen, Ye Li, *Low electromagnetic vibration design of double-layer interior permanent magnet machines for electric vehicle*, Energy Reports, vol. 7, Supplement 6, pp. 147–156 (2021), DOI: 10.1016/j.egyr.2021.08.062.

[10] Phi Hung Nguyen, Emmanuel Hoang, Mohamed Gabsi, *Bi-criteria optimization design of an interior permanent magnet synchronous machine for a hybrid electric vehicle application*, Mathematics and Computers in Simulation, vol. 90, pp. 178–191 (2013), DOI: 10.1016/j.matcom.2012.08.008.

[11] Huang J., Fu W., Niu S., Zhao X., Bi Y., Qiao Z., *A General Pattern-Based Design Optimization for Asymmetric Spoke-Type Interior PM Machines*, Energies, vol. 15, 9385 (2022), DOI: 10.3390/en15249385.

[12] Yong Kong, Da Xu, Mingyao Lin, *Efficiency modeling and comparison of surface and interior permanent magnet machines for electric vehicle*, Energy Reports, vol. 9, Supplement 1, pp. 419–426 (2023), DOI: 10.1016/j.egyr.2022.11.030.

[13] Pourahmadi-Nakhli M., Rahideh A., Mardaneh M., *Analytical 2-D Model of Slotted Brushless Machines with Cubic Spoke-Type Permanent Magnets*, IEEE Transactions on Energy Conversion, vol. 33, no. 1, pp. 373–382 (2018), DOI: 10.1109/TEC.2017.2726537.

[14] Mohammad M.R., Kim K.T., Hur J., *Design and analysis of a spoke type motor with segmented pushing permanent magnet for concentrating air-gap flux density*, IEEE Trans. Magn., vol. 49, no. 5, pp. 1035–1038 (2013), DOI: 10.1109/TMAG.2013.2240664.

[15] Mohammad M.R., Kim K.T., Hur J., *Design and optimization of neodymium-free spoke-type motor with segmented wing-shaped PM*, IEEE Trans. Magn., vol. 50, no. 2, pp. 865–868 (2014), DOI: 1109/TMAG.2013.2282151

[16] Boughrara K., Ibtiouen R., Takorabet N., *Analytic calculation of magnetic field and electromagnetic performances of spoke type IPM topologies with auxiliary magnets*, in Proc. Int. Conf. on Electr. Mach., pp. 51–57 (2014), DOI: 10.1109/ICELMACH.2014.6960158.

[17] Boughrara K., Ibtiouen R., Dubas F., *Analytical prediction of electromagnetic performances and unbalanced magnetic forces in fractional-slot spoke-type permanent-magnet machines*, in Proc. Int. Conf. Elect. Mach., pp. 1366–1372 (2014), DOI: 10.1109/ICELMACH.2016.7732702.

[18] Qiping S., Zhou Z., Li S., Liao X., Wang T., He X., Zhang J., *Design and Analysis of the High-Speed Permanent Magnet Motors: A Review on the State of the Art*, Machines, vol. 10, no. 7 (2022), DOI: 10.3390/machines10070549.

[19] Uler G.F., Mohammed O.A., Koh C.S., *Utilizing Genetic Algorithms for the Optimal Design of Electromagnetic Devices*, IEEE Transactions on Magnetics, vol. 30, no. 6, pp. 4296–4298 (1994), DOI: 10.1109/20.334066.

[20] Zhu Z., Zhu J., Zhu H., Zhu X., Yu Y., *Optimization Design of an Axial Split-Phase Bearingless Flywheel Machine with Magnetic Sleeve and Pole-Shoe Tooth by RSM and DE Algorithm*, Energies, vol. 13, 1256 (2020), DOI: 10.3390/en13051256.

[21] Ho S.L., Yang S., Ni G., Wong H.C., *A particle swarm optimization method with enhanced global search ability for design optimizations of electromagnetic devices*, IEEE Transactions on Magnetics, vol. 42, no. 4, pp. 1107–1110 (2006), DOI: 10.1109/TMAG.2006.871426.

[22] Chunyuan Liu, Rui Dong, Bao-lin Ye, *Comprehensive sensitivity analysis and multi-objective optimization on a permanent magnet linear generator for wave energy conversion*, Renewable Energy, vol. 198, pp. 841–850 (2022), DOI: 10.1016/j.renene.2022.08.102.

[23] Ho S.L., Yang S., Wong H.C., Cheng K.W.E., Ni G., *An Improved Ant Colony Optimization Algorithm and Its Application to Electromagnetic Devices Designs*, IEEE Transactions on Magnetics, vol. 41, no. 5, pp. 1764–1767 (2005), DOI: 10.1109/TMAG.2005.845998.

[24] Lucas S. Batista Felipe Campelo, Frederico G. Guimarães, Jaime A. Ramírez, Min Li, David A. Lowther, *Ant colony optimization for the topological design of interior permanent magnet (IPM) machines*,

The International Journal for Computation and Mathematics in Electrical and Electronic Engineering, vol. 33, iss. 3 (2014), DOI: 10.1108/COMPEL-08-2013-0285.

[25] Ho S.L., Yang S., Wong H.C., Ni G., *A Simulated Annealing Algorithm for Multiobjective Optimizations of Electromagnetic Devices*, IEEE Transactions on Magnetics, vol. 39, no. 3, pp. 1285–1288 (2003), DOI: 10.1109/TMAG.2003.810546.

[26] Fodorean D., Idoumghar L., N'diaye A., Bouquain D., Miraoui A., *Simulated annealing algorithm for the optimisation of an electrical machine*, IET Electric Power Applications, vol. 6, iss. 9, pp. 735–742 (2012), DOI: 10.1049/iet-epa.2011.0029.

[27] Basturk B., Karaboga D., *An Artificial Bee Colony (ABC) Algorithm for Numeric Function Optimization*, IEEE Swarm Intelligence Symposium, Indianapolis, USA (2006), DOI: 10.1007/s10898-007-9149-x.

[28] Greem Z.W., Kim J.H., Loganathan G.V., *A new heuristic optimization algorithm: harmony search*, Simulation, vol. 76, no. 2, pp. 60–68 (2001), DOI: 10.1177/003754970107600201.